PHYSICAL REVIEW E **90**, 032202 (2014)

Effect of volume fraction on granular avalanche dynamics

Nick Gravish and Daniel I. Goldman
School of Physics, Georgia Institute of Technology, Atlanta, Georgia 30332, USA

(Received 6 February 2014; published 3 September 2014)

We study the evolution and failure of a granular slope as a function of prepared volume fraction, ϕ_0. We rotated an initially horizontal layer of granular material (0.3-mm-diam glass spheres) to a 45° angle while we monitor the motion of grains from the side and top with high-speed video cameras. The dynamics of grain motion during the tilt process depended sensitively on $\phi_0 \in [0.58\text{–}0.63]$ and differed above or below the granular critical state, ϕ_c, defined as the onset of dilation as a function of increasing volume fraction. For $\phi_0 - \phi_c < 0$, slopes experienced short, rapid, precursor compaction events prior to the onset of a sustained avalanche. Precursor compaction events began at an initial angle $\theta_0 = 7.7 \pm 1.4°$ and occurred intermittently prior to the onset of an avalanche. Avalanches occurred at the maximal slope angle $\theta_m = 28.5 \pm 1.0°$. Granular material at $\phi_0 - \phi_c > 0$ did not experience precursor compaction prior to avalanche flow, and instead experienced a single dilational motion at $\theta_0 = 32.1 \pm 1.5°$ prior to the onset of an avalanche at $\theta_m = 35.9 \pm 0.7°$. Both θ_0 and θ_m increased with ϕ_0 and approached the same value in the limit of random close packing. The angle at which avalanching grains came to rest, $\theta_R = 22 \pm 2°$, was independent of ϕ_0. From side-view high-speed video, we measured the velocity field of intermittent and avalanching flow. We found that flow direction, depth, and duration were affected by ϕ_0, with $\phi_0 - \phi_c < 0$ precursor flow extending deeper into the granular bed and occurring more rapidly than precursor flow at $\phi_0 - \phi_c > 0$. Our study elucidates how initial conditions—including volume fraction—are important determinants of granular slope stability and the onset of avalanches.

DOI: 10.1103/PhysRevE.90.032202 PACS number(s): 45.70.Ht, 45.70.Cc, 45.70.Mg

Granular materials are collections of discrete particles that interact through repulsive contact forces [1–3]. These materials are of interest to physicists and engineers largely because of their ability to transition between fluidlike and solidlike states [2]. A granular avalanche is an important example of the granular solid-to-fluid transition. Avalanches of granular media are ubiquitous, occuring in industrial [4], laboratory [5], and natural settings (landslides).

The packing of a bed of granular material, measured by the prepared volume fraction, ϕ_0, may vary from loosely packed (low ϕ_0) to closely packed (high ϕ_0) initial conditions. ϕ_0 is defined as the ratio of solid volume to the occupied volume, and for relatively monodisperse particles $0.57 < \phi_0 < 0.64$ [3]. A granular material's resistance to flow is significantly affected by ϕ_0, as observed in boundary shear experiments [6–8], triaxial tests [9,10], and localized forcing by submerged objects [11–13]. In general, loosely packed granular material compacts when a shear stress or strain is applied while closely packed granular material dilates under shear [6]. The volume fraction at which the failure response of granular material transitions from compaction to dilation is called the granular critical state, ϕ_c, and it separates the two modes of granular failure under boundary-imposed forcing [6].

Little is known about how ϕ_0 influences the failure and avalanche onset of a dry granular slope. This is largely because in most granular avalanche experiments, the initial transient behavior is removed. For example, avalanche studies in continuously rotating drums [5,14–16], or particle deposition onto a slope [17], are typically performed in a steady state, such that transient behaviors are completed before observations are made. Thus in such experiments, the influence of ϕ_0 is not the focus of study.

An alternative method of investigating avalanche dynamics is through progressive loading. In such experiments, an undisturbed granular bed slowly rotates from a horizontal

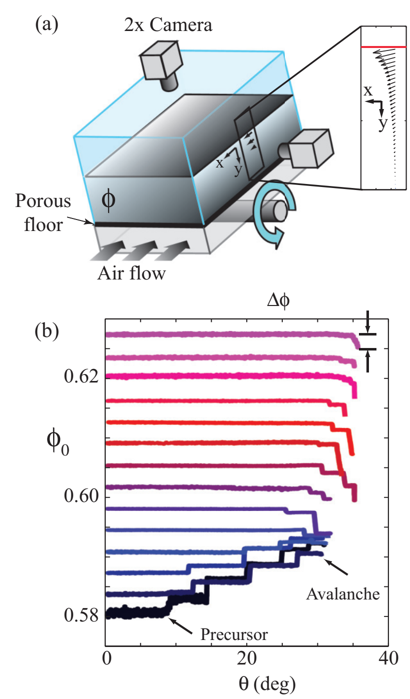

FIG. 1. (Color online) Experiment setup and volume fraction evolution during tilting of the granular bed. (a) Air flow through a porous floor in the fluidized bed and mechanical vibration prepare granular material to the desired initial ϕ. The bed rotates about midpoint and is imaged from the top and side views. The coordinate system is in the frame of reference of the rotating bed. (b) The average instantaneous volume fraction of the granular bed $\phi(t)$ vs tilt angle, θ, for 14 experiments at different ϕ_0. As the layer is inclined, compaction or dilation precursor events precede an avalanche. The preavalanche and failure dynamics are sensitive to initial ϕ_0.

orientation until an avalanche occurs [18]. In this way, granular materials can be prepared to a predetermined ϕ_0 prior to rotation. However, the majority of progressive loading experiments do not control ϕ_0. Progressive loading experiments typically performed at a single prepared $\phi_0 \approx 0.6$ (the "as-poured" state) have found that small rearrangements of the granular layer (precursors) precede the eventual surface avalanche onset [19–22]. Previously, volume fraction has been found to be an important determinant of the angle of maximum stability at which a granular avalanche begins [23]. Furthermore, a recent study of the precursor events in progressive loading of dry granular material reported that the intensity of these precursor events differed between two granular preparations, a densely and loosely packed initial state [22], suggesting an importance of ϕ on slope dynamics.

The effect of ϕ_0 on avalanche onset has been systematically studied in granular suspension experiments in which the granular material is immersed in a fluid. Results from these experiments [22,24,25] give an indication of what we may expect in dry granular materials: increasing ϕ_0 increases the angle of maximum stability. However, granular suspensions, with the presence of a viscous interstitial fluid, differ from dry granular materials. The feedback between fluid pore pressure and granular flow can be significant in suspension experiments, and can alter the mode of failure from that of dry granular materials. Additionally, frictional interactions among grains with an intermediate fluid may also differ from the dry case. A final difference between the previous suspension experiments and our current study is that the volume fractions realized in suspensions ($\approx$0.56–0.59) are typically lower than those of dry granular material ($\approx$0.57–0.64).

In this paper, we vary the prepared volume fraction of a dry granular material in experiment, and study the pre- and post-avalanche dynamics. We find that both pre- and post-avalanche behavior is sensitive to ϕ_0, and both exhibit a change in stability as ϕ_0 is increased above the critical state volume fraction, ϕ_c.

I. MATERIALS AND METHODS

An air fluidized bed of length $l = 43$ cm and width $w = 28$ cm was filled to a depth of $d \approx 9$ cm (bed height varied with packing condition) with a granular material of $D = 256 \pm 44$ μm diameter spherical glass beads [Fig. 1(a)]. Air flow through a porous rigid floor in the bed fluidized the granular material, and a combination of flow and mechanical vibration controlled the volume fraction as a function of vibration duration [12]. The volume fraction is defined as $\phi(t) = \frac{M}{\rho l w h(t)}$, where M is total grain mass, $\rho = 2.5$ g/cm^3 is grain density, and $h(t)$ is the time-varying height of the granular material. The prepared volume fraction is defined as $\phi_0 = \phi(t = 0)$. We varied the duration of mechanical vibration during granular state preparation to vary the initial ϕ_0 between $0.58 < \phi_0 < 0.63$. We defined the total change in volume fraction prior to the onset of an avalanche, $\Delta\phi = \phi_f - \phi_0$.

The experiments consisted of a constant rotation of the bed at angular speed 2.1 deg/s from an initial angle $\theta = 0^\circ$ to a final angle of $\theta = 45^\circ$. We performed similar experiments at lower rotation rates (down to 0.8 deg/s), but did not observe any significant change in avalanche dynamics. Two cameras recorded the granular motion during bed rotation. One camera mounted above the granular surface recorded grain motion at 30 Hz. A second camera was mounted on the side of the bed and imaged the granular material adjacent to the transparent wall at 200 Hz. The observation region of the side-view camera was 6×8 cm^2 (240×320 D^2) in height and width and the camera was centered in the middle of the length of the bed [see Fig. 1(a)]. We back-lit the granular bed such that the granular surface was detected as a high-contrast edge from black (grains) to white (background). To determine when flow occurred, we evaluated difference images between consecutive image frames. The pixel intensity in difference images did not map linearly to the amount of deformation that occurred between frames because the granular surface has similar texture features. However, difference images were a repeatable method of measuring when grain configurations changed, which we confirmed with follow-up particle image velocimetry experiments.

In additional experiments, we recorded video from the side at 1000 Hz; these images were used to find the velocity profiles of the particle flow at the sidewall through particle image velocimetry (PIV). This PIV method has been previously used in studying granular flows during plate drag [11,12]. Image resolution was 251 μm per pixel in both dimensions. We used a custom PIV algorithm that measured image correlations using the method of [26] with 1/10th subpixel resolution. We ignored PIV measurements at the surface where the stationary background hindered the correlation. We measured the depth-averaged PIV flow values for the horizontal and vertical granular flow directions over the depth range of 0–180 D.

The surface profile of the granular bed was tracked as a function of rotation angle over the duration of the experiment. The average height of the granular surface, $h(t)$, was used to compute the instantaneous mean volume fraction $\phi(t)$ by the equation given above. We defined θ_0 as the angle of the bed at which the first motion of the granular slope is observed. We define an avalanche as a continuous flow of granular material that resulted in a change in granular slope. θ_m was defined as the bed angle at which there occurred a continuous flow (lasting in duration greater than 1 s) in the material, which we defined as an avalanche. Lastly, θ_R is the repose angle of the granular material—the angle of the granular surface after the avalanche halts. We monitored the bed angle by recording the voltage drop across a potentiometer within the actuator.

II. ϕ-DEPENDENT SLOPE FAILURE

Granular slope response during tilting differed as a function of ϕ_0. At low ϕ_0, we observed that the slope underwent several compaction events—precursors—prior to the onset of avalanching flow [Fig. 1(b)]. Precursor compaction events were observed as a rapid increase in $\phi(t)$ and occurred intermittently throughout the tilting process and prior to the formation of an avalanche [Fig. 1(b)]. As ϕ_0 was increased, we observed that the tendency for granular precursors to occur prior to an avalanche diminished. At large ϕ_0, we found that the granular slope underwent dilation [a decrease in $\phi(t)$] immediately prior to avalanching flow at ϕ_f.

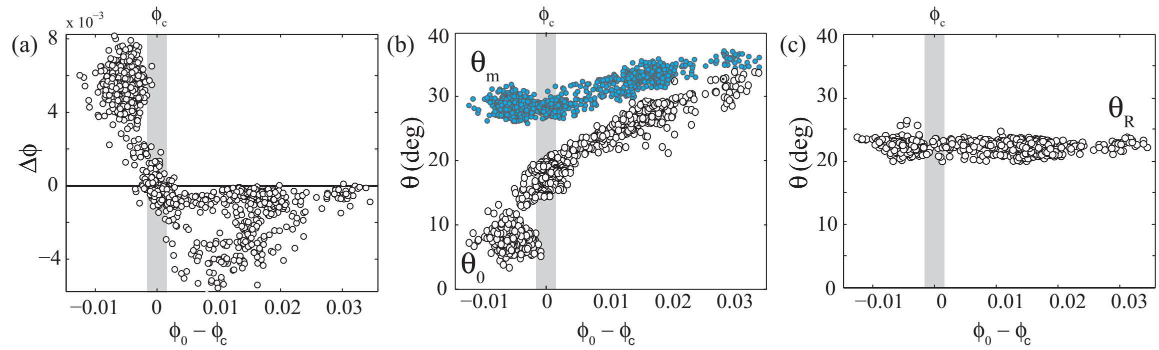

FIG. 2. (Color online) Avalanche dynamics. (a) Change in volume fraction $\Delta\phi$ is dependent on initial ϕ_0 and changed sign at $\phi_c = 0.595 \pm 0.003$. Each point in (a)–(c) represents a single experiment. Gray bar represents uncertainty in ϕ_c. (b) Initial angle of avalanche precursor, θ_0, and maximum angle of stability, θ_m, are sensitive to ϕ_0. (c) Angle of repose is insensitive to ϕ_0.

The total change in volume fraction from initial grain motion to the first avalanche is $\Delta\phi = \phi_f - \phi_0$. $\Delta\phi$ decreased from a positive value to a negative value as ϕ_0 increased. The critical state volume fraction where no dilation or compaction occurred was $\phi_c = 0.595 \pm 0.003$. Our measurement of ϕ_c is in accord with previous measurements made in plate drag experiments [11]. However, we note that the value of ϕ_c depends upon the material properties and the shape of the grains, in addition to the applied stresses on the grains [8], and thus varies across materials and experiments.

For $\phi_0 < \phi_c$, granular material compacted prior to the onset of an avalanche, and for $\phi_0 > \phi_c$, granular material dilated prior to the onset of an avalanche [Fig. 2(a)]. For $\phi_0 > \phi_c$, increasing ϕ_0 resulted in $\Delta\phi$ decreasing to a smaller yet still negative value. This indicated that the magnitude of dilation preceding an avalanche decreased with increasing ϕ_0. Such a decrease in $\Delta\phi$ likely occurs because higher ϕ_0 granular material experience larger internal stresses, which may inhibit volumetric expansion.

Both θ_0 and θ_m increased with increasing $\phi_0 - \phi_c$ [Fig. 2(b)]. Avalanche precursors occurred at low angles for low ϕ_0, with $\theta_0 = 7.7 \pm 1.4^\circ$ in the case of $\phi_0 - \phi_c = -0.006 \pm 0.001$. As $\phi_0 - \phi_c$ increased, so did θ_0, and for closely packed granular material, $\phi_0 - \phi_c = 0.032 \pm 0.001$, we observed $\theta_0 = 32.1 \pm 1.5^\circ$.

The bed angle at avalanche onset, θ_m, was also a function of $\phi_0 - \phi_c$ [Fig. 2(b)]. Increasing $\phi_0 - \phi_c$ increased θ_m from $\theta_m = 28.5 \pm 1.0^\circ$ to $35.9 \pm 0.7^\circ$ over the range of volume fractions observed. Although θ_m was sensitive to ϕ_0, the difference in magnitude of θ_m over the observed ϕ_0 was not as large as the variation observed in θ_0. We expect that the decreased sensitivity of θ_m on ϕ_0 is due to the series of precursor events that occur during the tilting process and prior to avalanche flow for $\phi_0 < \phi_c$, which likely strengthen the material. Our results for θ_m are in accord with a previous study of granular avalanches of Hostun sand, in which θ_m varied from $\approx 26^\circ$ to 37° over a range of five different initial packings from loose to close [23].

The final slope angle at which the granular material came to rest after the full 45° rotation is defined as the angle of repose, θ_R. Over the range of ϕ_0 observed, θ_R was independent of $\phi_0 - \phi_c$ [Fig. 2(c)], with a value of $\theta_R = 22 \pm 2^\circ$. The lack of dependence of θ_R on $\phi_0 - \phi_c$ indicates that due to the grain motion prior to and during an avalanche the granular material evolves to a critical state, independent of its previous state [6]. The independence of θ_R on prepared volume fraction is evidence that θ_R is a property of the granular material, dependent only on the grain mechanical properties (coefficient of friction, restitution, shape, etc.) [27].

The angle of repose we observe for dry, spherical glass beads is consistent with previous observations [28]. Additionally, the values of θ_m we observe are consistent with the ranges reported in previous experiments on similar granular material [28]. However, our observations of granular motion at tilt angles lower than $\theta_0 < 10^\circ$, which occur at low $\phi_0 - \phi_c$, have not been observed in previous granular avalanche experiments. It is likely that in previous experiments in which $\phi_0 - \phi_c$ was not varied, the volume fraction was near ϕ_c and was in the "as-poured" granular state. The dynamics of failure and flow away from ϕ_c are less understood, and our results shed light on this phenomenon.

III. GRANULAR FLOW AT FAILURE

To characterize the granular flow during the precursor events at varying θ_0, we computed the flow profile at a sidewall using PIV (Fig. 3). Since precursor events consisted of a flow initiation and flow arrest, we measured the displacement field of the granular flow $[d_x(y),d_y(y)]$ along a vertically oriented line centered in the imaging region and in the reference frame of the tilted bed. The displacement field of the granular flow during the first precursor depended on $\phi_0 - \phi_c$. In loose granular media [$\phi_0 - \phi_c < 0$; see Fig. 3(a)], flow resulted in material displacement parallel to and down the length of the bed [positive $d_x(y)$], and a vertical displacement toward the floor of the enclosure [positive $d_y(y)$]. Positive $d_y(y)$ indicates a compaction of the granular material as expected for $\phi_0 - \phi_c < 0$. When the granular material was prepared near the critical state, $\phi_0 - \phi_c \approx 0$ [Fig. 3(b)], $d_x(y)$ decreased and $d_y(y)$ approached zero as compared to the loose pack state. This indicated that no compaction or dilation occurred during failure onset—the definition of the granular critical state. Lastly, in the dilating regime, $\phi_0 - \phi_c > 0$ [Fig. 3(c)], $d_x(y)$ decreased as ϕ_0 increased and $d_y(y)$ was negative and decreased with increasing ϕ_0. In general, the vertical grain motion during a precursor was in the downward direction (compacting) for $\phi_0 - \phi_c < 0$ and in the upward direction (dilating) for $\phi_0 - \phi_c > 0$.

From the displacement profiles of the precursor flow, we now evaluate quantitative differences in granular response in the dilating or compacting regimes. We measured the depth-averaged mean displacement of the horizontal and vertical granular flow, $\langle d_i \rangle$ ($i = x,y$), averaged over depths 0–180 D (Fig. 4). With increasing ϕ_0, $\langle d_x \rangle$ decreased in magnitude and $\langle d_y \rangle$ decreased from positive to negative values and crossed zero at ϕ_c [Figs. 4(a) and 4(b)], as expected from the definition of the critical state. The difference in magnitude of $\langle d_y \rangle$ and $\langle d_x \rangle$ across ϕ_c demonstrates that material at low ϕ_0 is susceptible to large displacements during failure as compared to high ϕ_0. At higher volume fractions—above ϕ_c—initial grain motion resulted in comparatively small displacements during precursor failure [Figs. 4(a) and 4(b)].

The dilation that occurs per unit shear in a granular material is measured by the tangent of the dilatancy angle, ψ [Fig. 4(c)]. For our geometry, we assume translational invariance along the horizontal direction (x in the frame of the rotating bed), similar to a simple-shear flow. The dilatancy angle therefore is the angle the displacement vector of the surface deformation makes with the horizontal. In the case of simple shear, we may estimate the dilatancy angle as $\tan(\psi) = \frac{\langle d_y \rangle}{\langle d_x \rangle}$ averaged over the entire depth of the flow. We plot $\tan(\psi)$ as a function of $\phi_0 - \phi_c$ [Fig. 4(c)] and we find that the dilatancy angle during precursor failure obeys the equation $\tan(\psi) = K(\phi_0 - \phi_c)$, where $K = 22.4 \pm 2.4$. This relationship was originally introduced by Roux *et al.* [29] and is effectively a linearization of the function $\psi(\phi_0 - \phi_c)$ about the critical state $\phi_0 - \phi_c = 0$.

To gain insight into the values of $\tan(\psi)$ observed in experiment, we construct a simple scenario of dilating and compacting flow. We imagine a two-dimensional arrangement of diameter D spheres in a square lattice (loose-packing) or a hexagonal lattice (close-packing). In both cases, we impose a lateral displacement, d_x, and we compute the resultant d_y of the grain layer [see the drawings in Fig. 4(c)]. In both cases, for a lateral displacement of $d_x = \frac{D}{2}$, the grains must displace

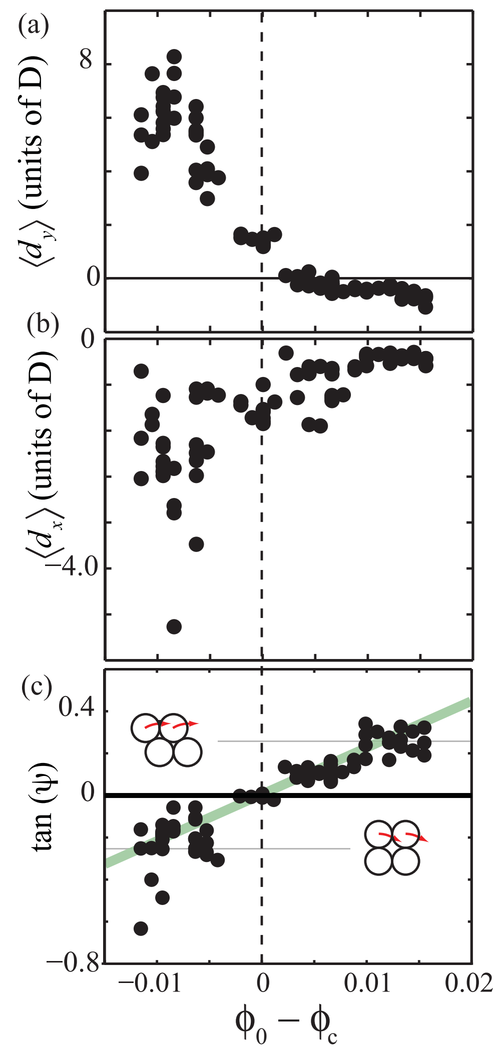

FIG. 4. (Color online) Mean granular displacement during precursor avalaching. (a) and (b) Depth-averaged vertical ($\langle d_y \rangle$) and horizontal ($\langle d_x \rangle$) displacement of granular material at different prepared $\phi_0 - \phi_c$. (c) Tangent of the dilation angle, ψ, vs $\phi_0 - \phi_c$. Horizontal lines correspond to close- and loose-packed examples described in the text.

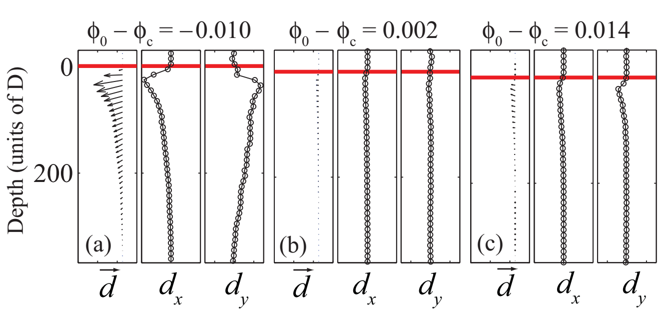

FIG. 3. (Color online) Profiles of granular displacement during precursor failure. Displacement profiles of a loose-packed (a), a critical (b), and a close-packed (c) granular material shown from left to right. For each initial condition, we show a vector displacement field of flow, x displacement (d_x), and y displacement (d_y). The red line indicates surface location. The vector field is in the rotating frame of reference of the granular bed, and the downslope direction is to the left.

maximally vertically $d_y = 0.134$ in the $\pm y$ direction, resulting in $\tan(\psi) = \pm 0.268$ [where by definition (−) is dilation]. The peak dilation and compaction observed in experiment are close to the values of $\tan(\psi)$ predicted from the simple scenario presented above, which gives some insight into the magnitude of compaction (dilation) that the loose (close) pack undergoes in experiment [see the gray lines in Fig. 4(c)]. Larger and smaller values of $\tan(\psi)$ are likely due to the disordered nature of the granular configurations created in experiment.

Finally, we compare our results on dry granular materials to those on granular suspensions performed by Pailha *et al.* [24]. They observed a similar linear relationship between ϕ_0 and $\tan(\psi)$ [Fig. 4(c)], with fit parameters of $K = 3.4$ and $\phi_c = 0.582$. The lower value of ϕ_c observed in [24] is likely due to the hydrostatic fluid pressure in their experiments, which reduces internal granular stresses and thus reduces ϕ_c [8]. A lower value of K indicates that for comparable horizontal grain

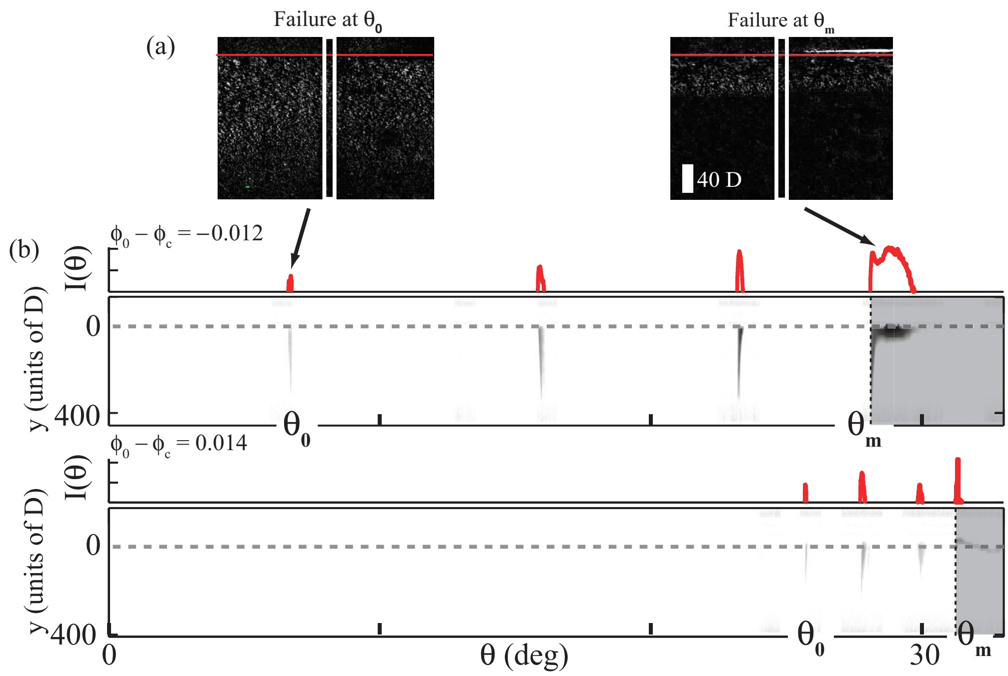

FIG. 5. (Color online) Spatiotemporal evolution of granular flow during slow tilting of the bed. (a) Difference images of granular flow at θ_0 (left) and θ_m (right). The red line indicates the top surface. White spots correspond to regions that underwent a rearrangement of particle positions. The white vertical rectangle in the center illustrates the region plotted vs time below. (b) Space-rotation angle profiles of granular flow generated by evaluating image differences along a vertical strip in the image center over time [white rectangle in (a)]. Gray-scale signifies the intensity of pixel differences shown in (a), however gray-scale intensity does not map linearly to granular displacement (see Sec. I). The intensity plots of the flow profile are shown above the space-rotation angle plots (arbitrary units). Top plots are loose pack and show a precursor event occurring at $\theta_0 = 6.2^\circ$. Several precursors occur prior to the initiation of a surface avalanche at $\theta_m = 28.1^\circ$ (gray regions signify avalanche regime).

motion, less vertical motion is experienced in the granular suspension compared to the dry granular material. The smaller vertical motion in the fluid-immersed experiments [24] is likely due to the resistive influence of the pore pressure from the surrounding viscous fluid. For instance, a suction pressure is generated when a fluid-immersed granular material dilates, generating higher grain-grain stresses that in turn may resist the dilation motion, and thus lower d_y.

IV. ϕ_0 DEPENDENCE ON FLOW DEPTH

During the granular flow at θ_0, we observed that the flow profile extended deeper into the granular layer than during avalanche flow at θ_m. We observed this by computing image differences of successive video frames from high-speed video (1000 Hz) of the progressive loading experiment [Fig. 5(a)]. We visualized the dynamics of the avalanche process by examining the space-time evolution of the image difference magnitude, evaluated along a thin vertical strip centered in the observation region [white boxes in Fig. 5(a)]. We constructed space-time images by plotting the intensity of difference images (time interval of 1 ms) at depth, y, and time, t, within this thin strip. Image difference profiles for high and low ϕ_0 showed intermittent precursor events at $\phi_0 - \phi_c < 0$ prior to an avalanche [Fig. 5(b)]. As ϕ_0 increased, the angle at which the precursor flow occurred also increased.

The space-time evolution of individual precursor events varied in shape and size as a function of $\phi_0 - \phi_c$ [Figs. 6(a) and 6(b)]. We observed that precursor events either initiated from the surface and propagated downward [Fig. 6(a)] or occurred simultaneously throughout the layer [Fig. 6(b)]. However, we did not observe a systematic dependence of this behavior on $\phi_0 - \phi_c$. In the example shown in Fig. 6(a), in which the flow-front propagated downward, the propagation speed of the compaction front was $v = 1.08$ m/s. For comparison, the speed of sound propagation in granular material is ≈280 m/s [30] and the speed of sound in glass is ≈4000 m/s.

Although the spatiotemporal evolution of the precursor flow did not vary with $\phi_0 - \phi_c$, the magnitude of spatiotemporal flow events varied with $\phi_0 - \phi_c$ in both maximum depth (d_a for avalanche depth and d_p for precursor avalanche depth), and precursor flow duration, ΔT [Figs. 6(c) and 6(d)]. ΔT, was a nonmonotonic function of $\phi_0 - \phi_c$ and increased to a maximum near ϕ_c [Fig. 6(c)]. Precursor depth was sensitive to $\phi_0 - \phi_c$ and was approximately constant, $d_p = 320 \pm 2.4$ D, for $\phi_0 - \phi_c < 0$ and linearly decreasing, $d_p = (-968\ \mathrm{D})\phi_0 + 33$ D, for $\phi_0 - \phi_c > 0$ [Fig. 6(d)]. The functional difference in $d_p(\phi_0)$ as ϕ_0 exceeds ϕ_c is another signature of a bifurcation in the granular rheology that occurs at the dilation transition [11].

The avalanche depth, $d_a = 45 \pm 17$ D, was significantly shallower than the precursor events [Fig. 6(d)] and was independent of $\phi_0 - \phi_c$. The independence of d_a as a function of $\phi_0 - \phi_c$ suggests that fully formed avalanche flow is not dependent upon the prior initial state. Insensitivity of avalanche depth likely occurs because grain rearrangements prior to

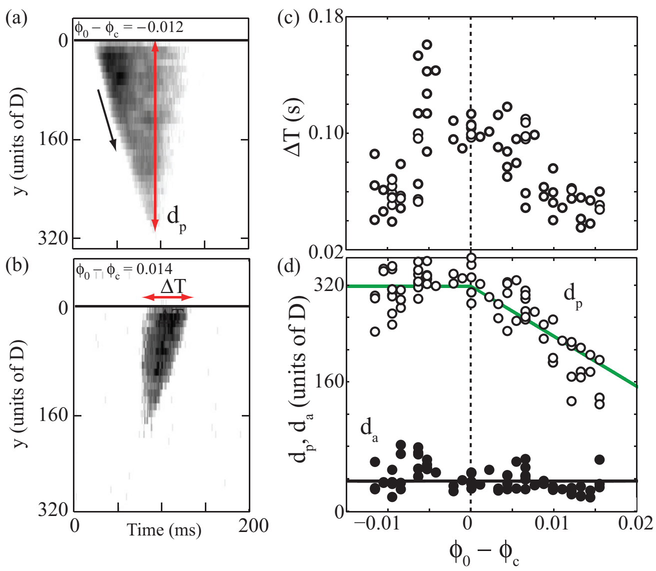

FIG. 6. (Color online) Spatiotemporal evolution of granular flow during precursors and avalanches. (a) and (b) Space-time images of precursor events at θ_0 in a loose- (a) and close- (b) packed granular media. In example (a), flow begins at the surface and propagates vertically into the granular layer (black arrow) at a speed of approximately $v = 1.08$ m/s, to a maximum depth d_a. In example (b), flow begins simultaneously throughout the layer. The intensity of the image is arbitrary and chosen to highlight flow shape. (c) Time duration of precursor events as a function of $\phi_0 - \phi_c$. (d) Depth dependence of precursor and avalanche flow as a function of initial $\phi_0 - \phi_c$. White circles are precursor flow and black circles are avalanching flow. The black and green lines show the fit functions described in the text.

avalanche formation act to compact or dilate the granular material toward the critical state, independent of ϕ_0.

V. CONCLUSION

Understanding the conditions that lead to failure of a granular slope have important applications in diverse fields such as bridge and dam design, the development of rugged robots [31] and extraterrestrial rovers [32], and the biology of sand-dwelling organisms [33]. In our experimental investigation of the effect of volume fraction on the failure of a granular slope, we found that slope failure differed significantly as a function of initial ϕ_0.

Response of the granular media to our progressive loading experiment was divided into roughly two regimes, above or below ϕ_c. Below ϕ_c, the granular material underwent several compaction events prior to the onset of sustained surface flow defined as an avalanche. The angle at which compaction precursor events began in the case of the lowest ϕ_0 occurred at $\theta_0 = 7.7 \pm 1.4^\circ$, a value of slope failure substantially lower than what has been observed in previous avalanche experiments with "as-poured" granular material in which volume fraction is not typically varied. As ϕ_0 was increased, we observed an increase in θ_0, which approached the maximum angle of stability, θ_m, as ϕ_0 increased. The value of θ_m we observed for the critical state, ϕ_c, was consistent with values observed for similar glass particles prepared in an "as-poured" state or subject to multiple avalanches in rotating drum experiments [28]. We emphasize that, as in previous experiments [8,11,13,23,34], ϕ_0 plays an important role in granular flow in response to stress.

ACKNOWLEDGMENTS

Funding was provided by the Burroughs Wellcome Fund, ARL MAST CTA, ARO Grant No. W911NF-11-1-0514, and NSF Physics of Living Systems. We thank Azeem Bande-Ali for his help with the data collection and analysis.

[1] H. M. Jaeger and S. R. Nagel, Science **255**, 1523 (1992).
[2] H. M. Jaeger, S. R. Nagel, and R. P. Behringer, Rev. Mod. Phys. **68**, 1259 (1996).
[3] R. Nedderman, *Statics and Kinematics of Granular Materials* (Cambridge University Press, Cambridge, 1992), p. 352.
[4] S. P. Pudasaini and K. Hutter, *Avalanche Dynamics: Dynamics of Rapid Flows of Dense Granular Avalanches* (Springer, Berlin, 2007).
[5] Y. Forterre and O. Pouliquen, Annu. Rev. Fluid Mech. **40**, 1 (2008).
[6] A. Schofield and P. Wroth, *Critical State Soil Mechanics* (McGraw-Hill, London, 1968).
[7] E. Aharonov and D. Sparks, Phys. Rev. E **60**, 6890 (1999).
[8] C. Wroth, Engineering **186**, 409 (1958).
[9] M. Oda and H. Kazama, Geotechnique **48**, 465 (1998).
[10] S. Fazekas, J. Török, and J. Kertész, Phys. Rev. E **75**, 011302 (2007).
[11] N. Gravish, P. B. Umbanhowar, and D. I. Goldman, Phys. Rev. Lett. **105**, 128301 (2010).
[12] N. Gravish, P. B. Umbanhowar, and D. I. Goldman, Phys. Rev. E **89**, 042202 (2014).
[13] M. Schröter, S. Nägle, C. Radin, and H. L. Swinney, Europhys. Lett. **78**, 44004 (2007).
[14] D. Khakhar, J. McCarthy, T. Shinbrot, and J. Ottino, Phys. Fluids **9**, 31 (1997).
[15] G. MiDi, Eur. Phys. J. E **14**, 341 (2004).
[16] X. Y. Liu, E. Specht, and J. Mellmann, Powder Technol. **154**, 125 (2005).
[17] V. Frette, K. Christensen, A. Malthe-Sørenssen, J. Feder, T. Jøssang, and P. Meakin, Nature (London) **379**, 49 (1996).
[18] M. Bretz, J. B. Cunningham, P. L. Kurczynski, and F. Nori, Phys. Rev. Lett. **69**, 2431 (1992).
[19] L. Staron, F. Radjai, and J.-P. Vilotte, J. Stat. Mech.: Theor. Exp. (2006) P07014.
[20] S. K. de Richter, G. Le Caër, and R. Delannay, J. Stat. Mech.: Theor. Exp. (2012) P04013.
[21] V. Y. Zaitsev, P. Richard, R. Delannay, V. Tournat, and V. Gusev, Europhys. Lett. **83**, 64003 (2008).

[22] A. Amon, R. Bertoni, and J. Crassous, Phys. Rev. E **87**, 012204 (2013).

[23] P. Evesque, D. Fargeix, P. Habib, M. P. Luong, and P. Porion, Phys. Rev. E **47**, 2326 (1993).

[24] M. Pailha, M. Nicolas, and O. Pouliquen, Phys. Fluids **20**, 111701 (2008).

[25] F. Bonnet, T. Richard, and P. Philippe, Granular Matter **12**, 317 (2010).

[26] M. Guizar-Sicairos, S. T. Thurman, and J. R. Fienup, Opt. Lett. **33**, 156 (2008).

[27] H. Matuttis, S. Luding, and H. Herrmann, Powder Technol. **109**, 278 (2000).

[28] R. Albert, I. Albert, D. Hornbaker, P. Schiffer, and A.-L. Barabási, Phys. Rev. E **56**, R6271(R) (1997).

[29] S. Roux and F. Radjai, *Physics of Dry Granular Media*, NATO ASI Series Vol. 350 (Springer, Netherlands, 1998), pp. 229–236.

[30] C.-h. Liu and S. R. Nagel, Phys. Rev. Lett. **68**, 2301 (1992).

[31] C. Li, P. B. Umbanhowar, H. Komsuoglu, D. E. Koditschek, and D. I. Goldman, Proc. Natl. Acad. Sci. (USA) **106**, 3029 (2009).

[32] F. Zhou, R. E. Arvidson, K. Bennett, B. Trease, R. Lindemann, P. Bellutta, K. Iagnemma, and C. Senatore, J. Field Robotics **31**, 141 (2014).

[33] N. Mazouchova, N. Gravish, A. Savu, and D. I. Goldman, Biol. Lett. **6**, 398 (2010).

[34] P. Umbanhowar and D. I. Goldman, Phys. Rev. E **82**, 010301 (2010).